Journal of Catalysis **212,** 136–144 (2002)
doi:10.1006/jcat.2002.3742

Mechanisms for Chain Growth in Fischer–Tropsch Synthesis over Ru(0001)

I. M. Ciobîcă,*,[1] G. J. Kramer,* Q. Ge,† M. Neurock,† and R. A. van Santen*

*Schuit Institute of Catalysis, Eindhoven University of Technology, P.O. Box 513, 5600 MB Eindhoven, The Netherlands; and †Department of Chemical Engineering, University of Virginia, Charlottesville, Virginia 22903-2442

Received January 8, 2002; revised June 5, 2002; accepted June 19, 2002

Two reaction pathways for hydrocarbon chain-growth mechanisms over Ru(0001) in Fischer–Tropsch synthesis have been analyzed using periodic *ab initio* calculations for 25% coverage. Adsorption energies for the intermediates for the first two catalytic cycles for each mechanism as well as the transition states are reported. Both mechanisms are carbene-type mechanisms. Adsorbed CH species are used as the building unit, rather than adsorbed CH_2 intermediates. The resulting intermediate hydrocarbon chains at the surface are alkyl- and alkylidenelike, respectively.

Key Words: **Fischer–Tropsch mechanism; molecular modeling, DFT; Ru(0001) surface; transition states.**

1. INTRODUCTION

There has been a resurgence in the interest of Fischer–Tropsch synthesis over the past few years in an effort to selectively engineer the resulting molecular product distributions that form (1–4). This would significantly impact the development of ultraclean fuels. Abundant methane sources, advances in methane activation chemistry, and novel reactor technology have helped to drive much of this renewed interest (5–10). Fischer–Tropsch synthesis involves a complex reaction scheme composed of myriad different reactive intermediates and elementary reaction paths. The general overall reaction paths include CO activation, C_xH_y hydrogenation, hydrocarbon coupling, and termination pathways. Over 40 years of outstanding research effort has helped to resolve many important issues concerning the overall reaction chemistry. The controlling reaction mechanism, however, is still actively debated. The following three mechanisms have been proposed and debated for quite some time:

- the carbene mechanism.
- the hydroxy-carbene mechanism.
- the CO-insertion mechanism.

In the carbene mechanism, CO and hydrogen dissociate over supported metal particles to form surface carbon and hydrogen. Carbon adatoms go on to readily hydrogenate to form CH, CH_2, and/or CH_3 intermediates. These intermediates can then couple to form longer chain hydrocarbons. Chain termination proceeds by (a) dehydrogenation of one of the growing chains to form a terminal olefin, (b) hydrogenation of the C_xH_y intermediates to form a paraffin, or (c) disproportionation of C_xH_y intermediates to form either olefins or paraffins.

In the hydroxy-carbene mechanism, it is thought that two neighboring CO intermediates react with hydrogen to form two reactive hydroxy carbene intermediates. The addition of hydrogen and subsequent elimination of water from these adsorbed RCHOH intermediates leads to the formation of a growing hydrocarbon chain.

The CO insertion mechanism is characteristically different from the previous two mechanisms in that CO remains intact. Hydrocarbon coupling proceeds via the insertion of CO into surface hydrocarbon intermediates to form C_xH_yO intermediates. The terminal oxygen is ultimately removed by the hydrogenation of the surface C_xH_yO oxygenate and the desorption of water.

Spectroscopic evidence indicates that CO is reduced to elemental carbon and subsequently converted to CH and CH_2 intermediates (11–14). Model experiments also show that CH_2 intermediates can easily form and subsequently react to form longer chain hydrocarbons. The carbene mechanism appears to have the greatest following.

While evidence suggests that CO activation may be a rate-limiting process, the product distribution that forms, however, is controlled by the balance between hydrogenation steps, hydrocarbon coupling, and termination steps.

We have used *ab initio* quantum chemical calculations to complement previous experimental efforts and to offer more atomic-level description of how specific steps can take place. In previous papers, we have discussed potential adsorption sites and reaction paths for CO activation (15) and C_1H_x hydrogenation over Ru (16, 17) in great detail. In this work, we examine hydrocarbon coupling steps. More specifically we focus on the initial C_1 and C_2 coupling steps in order to understand which sites and species are likely involved and how the elementary steps proceed.

[1] To whom correspondence should be addressed. E-mail: i.m.ciobica@tue.nl.

0021-9517/02 $35.00

We examine two different propagation cycles that follow different arrangements of hydrocarbon coupling and hydrogenation steps over Ru. The two mechanisms proposed help to explain the formation of both saturated and unsaturated long-chain hydrocarbons. We use theory to calculate the activation barriers as well as the overall reaction energies for each of the CH_x coupling steps involved in the two sequences. This provides an initial basis toward determining which of these processes is more likely. While hydrocarbon coupling is critical to the chain propagation and the distribution of products that ultimately form, it is balanced by the hydrogenation and chain termination steps. A more complete test of which intermediates control FT chemistry will ultimately involve simulating the full spectrum of elementary steps, including CO activation, hydrogenation, chain coupling, and chain termination.

2. CHEMISORPTION OF C_xH_y INTERMEDIATES ON TRANSITION METALS

C_1H_y and C_2H_y intermediates are at the heart of hydrocarbon coupling for FT synthesis. In addition, they are also of interest due to their formation in alkane activation processes and other hydrocarbon conversion chemistries (5, 6, 9, 10). Several *ab initio* theoretical studies on the chemistry of alkanes and other C_xH_y intermediates over transition metal surfaces have recently been published. We report on these results due to their relevance to the work described herein.

Papoian *et al.* (18) used periodic density functional theory to examine the chemisorption of H, CH_3, and C_2H_5 species on the 2×2 Pt(111) surface. They found that while there was no clear preference for the adsorption site of atomic hydrogen, the hydrocarbon analogs CH_3 and C_2H_5 favor the atop adsorption sites. Chemisorption at the bridge and threefold sites were found to be unfavorable.

Kua and Goddard (19, 20) also studied the chemisorption of C_2H_x and CH_x species on model Pt(111) surfaces. They used nonlocal gradient corrected DFT calculations on model Pt clusters to infer information on the chemisorption energies. Methyl was found to prefer the atop adsorption site, methylene preferred the bridge site, and CH and C preferred the threefold hollow sites. The CH intermediate was found to be the most stable intermediate in the CH_x series. In moving to the C_2H_x intermediates ethyl was found to adsorb atop, ethylidene on the bridge sites, ethylene in a di-σ adsorption mode, vinyl in the η1η2 adsorption configuration over the threefold site, acetylene in a tetra-σ configuration at the threefold site, and vinylidene at the threefold hollow site. CCH and CC adsorb with the C–C bound tilted; one C sits above the hollow site and the other sits atop. The most stable species from the C_2H_x series was ethylidyne, which adsorbed at the threefold hollow site. This was followed by acetylene, vinyl, and ethylene. The CCH and CC were found to be the most unstable. All of the CH_x and C_2H_x species appeared to follow the classical octet rule, thus forming four σ bonds.

Watwe *et al.* (21) also studied the stability of C_2H_x adspecies on Pt(111) as well as on Pt(211) surfaces. They performed both cluster and periodic slab calculations. They found similar results in that the C_2H_x intermediates bind to sites that preserve the tetrahedral geometry and saturate the coordination of the carbon atoms in the adsorbed C_2H_x species. The authors also calculate transition states for C–C bond dissociation. The easiest bonds to break are the carbon–carbon bonds for ethylidene adsorbed to Pt(111) and the C–C bonds of vinyl adsorbed on Pt(211). The most difficult bonds to break are the CH_2–CH_2 bonds for ethylene on both the Pt(111) and Pt(211) surfaces.

Finally, Pallassana and Neurock (22) reported on the hydrogenation and dehydrogenation pathways for C_2H_x intermediates over Pd. These results also indicate that each of the carbon atoms in the C_2H_x intermediate attempts to preserve the octet rule by forming four bonds. The number of bonds formed with the surface can be found by simply subtracting the number on hydrogen atoms to specific carbon atom and the number of bonds to carbon (one for a sigma bond, two for a double bond) from the value of four. The results indicate the following ordering in terms of the strength of chemisorption and its relationship to the number of metal–carbon bonds:

CH_3–CH_3 (MC = 0) < CH_3–CH_2– (MC = 1) < CH_3–CH– (MC = 2) < CH_3–C– (MC = 3).

The most stable species is ethylidyne, which forms three bonds to the surface and one to carbon.

These results provide a basis for understanding the nature of absorption and reactivity of the CH_xCH_y intermediates and a database for comparison for the calculations presented herein on the Ru(0001) surface.

3. METHOD AND SURFACE MODEL

All calculations reported herein were performed using plane wave periodic density functional theoretical calculations as implemented in the Vienna Ab Initio Simulation Package VASP (23, 24) code. Generalized gradient corrections were carried out using the Perdew–Wang 91 functional (25). The smearing method of Methfessel and Paxton (26) was applied to help with the convergence of the self-consistent field. The free energy here is a variational quantity and the energy is subsequently extrapolated for σ = 0.0 eV. The interactions between the ions and the electrons are described by the Vanderbilt ultrasoft pseudopotentials (US-PP) (27) provided by Kresse and Hafner (28).

The supercell consists of a four-layer slab with seven vacuum layers between the slabs, in a 2×2 supercell. Adsorption on both sides with an inversion center prevents

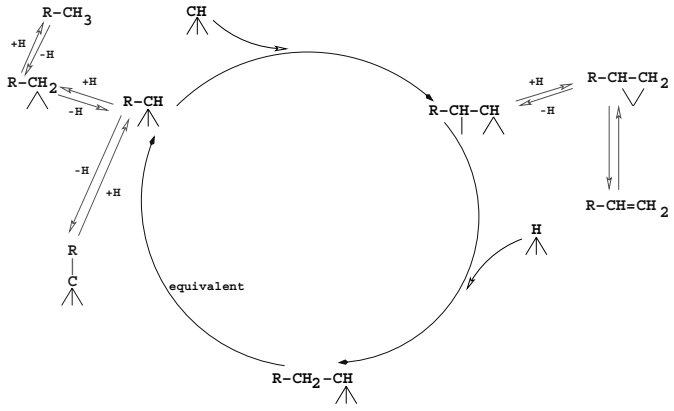

FIG. 1. Fischer–Tropsch, mechanism 1. | indicates atop adsorption, ∧ indicates bridge adsorption, ⩚ indicates threefold site (fcc or hcp) adsorption, and ∨ indicates di-σ adsorption mode. The R is H for the first cycle and CH_3 for the second one.

the generation of dipole–dipole interactions between the supercells. The *k*-points sampling was generated following the Monkhorst–Pack procedure (29) with a $5 \times 5 \times 1$ mesh. The 3×3 supercell also has a four-layer slab with five vacuum layers between the slabs. The *k*-points sampling used a $3 \times 3 \times 1$ mesh.

The cutoff energy for the plane waves basis set is 300.0 eV. The coordinates of all of the atoms were fully optimized. All the parameters (the *k*-points mesh, the number of metal and vacuum layers, etc.) were tested and carefully selected (16).

The nudged elastic band (NEB) method developed by Jónsson *et al.* (30) is used to determine the transition states reported herein. This is a chain-of-states method. Two points in the hyperspace containing all the degrees of freedom are needed (initial and final state) and a linear interpolation can be made to produce the images along the elastic band. The program will run simultaneously for each image and will communicate at the end of each ionic cycle in order to compute the force acting on each image.

The term "nudged" indicates that the projection of the parallel component of true force acting on the images and the perpendicular component of the spring force are canceled. A smooth switching function is introduced that gradually turns on the perpendicular component of the spring force where the path becomes kinky at large differences in the energies between images.

The results obtained with the NEB are refined with a quasi-Newton algorithm (31). This implies that the atoms are moved in such a way as to minimize the forces. The total energy is not taken into account for minimization. In this way the program is searching for a stationary point. Only in the very few cases where the given initial geometry is close to the geometry of the TS is it possible to reach the TS directly with the quasi-Newton technique, so the NEB is still required.

4. RESULTS AND DISCUSSION

We carried out a systematic study of the chemisorption and the stability of different C_2H_x intermediates on the Ru(0001) surface. The results were reported in detail in a previous communication (32). We highlight just a few of the important findings here because of their relevance in mapping out the reaction paths for hydrocarbon coupling.

CH was found to be the most stable of all C_1 surface intermediates. This would suggest that CH is the dominant surface species rather than CH_2 under the conditions reported here. This, of course, will depend on the balance between the rate of hydrogenation versus the rate of hydrocarbon coupling. The rates as well as the stability of these intermediates can change as we move to different surface structures and different metals. Experiments, for example, show that CH_2 is the most stable intermediate on the Ru(11$\bar{2}$0) surface and the theory that supports it (33).

The results from our *ab initio* calculations for methane activation were used in a dynamic Monte Carlo simulation algorithm to establish the most abundant surface intermediate for methane activation and C_1 hydrogenation (34, 35). The CH adspecies was found to be present under most conditions. CH_2 species do begin to form in greater abundance at higher surface coverages.

In the work discussed herein, CH is used as the primary monomer unit for growing longer hydrocarbon chains. While CH_2 is examined as a potential reaction species, we do not consider it here to be a monomeric building unit. We probe two different hydrocarbon coupling cycles. The first examines the addition of CH to a growing alkylidene chain. This mechanism leads to the formation of a homologous series of R–C–H intermediates, including CH_2, CH_3CH, and CH_3CH_2CH, as shown in Fig. 1 (mechanism 1).

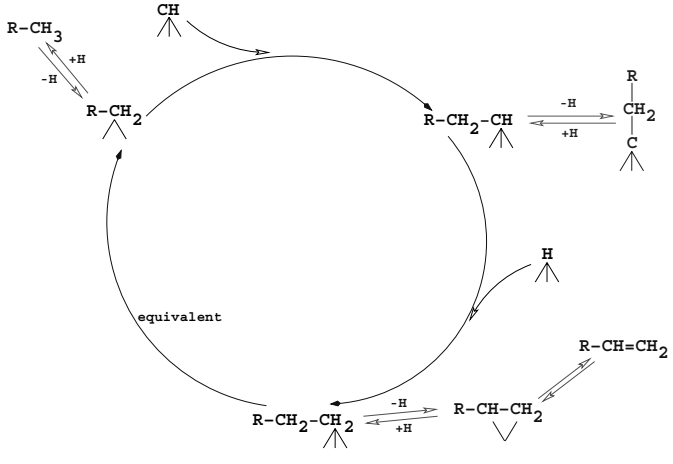

FIG. 2. Fischer–Tropsch, mechanism 2. | indicates atop adsorption, ∧ indicates bridge adsorption, ⩚ indicates threefold site (fcc or hcp) adsorption, and ∨ indicates di-σ adsorption mode. The R is H for the first cycle and CH_3 for the second one.

The second cycle involves the addition of CH to a growing alkyl chain. This mechanism leads to the formation of a homologous series of alkyl intermediates, including CH_3, CH_3CH_2, and $CH_3CH_2CH_2$, as shown in Fig. 2 (mechanism 2). We do not, however, consider the addition of CH to a growing alkylidyne chain (CH_3C, CH_3CH_2C, etc.) which was proposed by Maitlis *et al.* (36). Both the CH and the alkylidyne intermediates are strongly bound to the surface, making it difficult for them to react together. The barriers for hydrogenation are also believed to be very high due to their unfavorable reaction enthalpy.

The alkylidene mechanism shown in Fig. 1 starts with an adsorbed R–CH intermediate. In the first pass through the cycle R–CH is equal to CH_2. R–CH subsequently reacts with an adsorbed CH building unit. The result is an adsorbed R–CH–CH vinyllike intermediate. RCH–CH adsorbs with its terminal CH group attached to a bridge site and its adjacent secondary CH group bound to an atop Ru site. This is referred to as η1η2 3-σ adsorption. This vinyllike intermediate can then be hydrogenated to form an adsorbed alkene, which can either desorb or hydrogenate to form an $R–CH_2–CH$ intermediate. The $R–CH_2–CH$ alkylidene intermediate is the homologue of the species which initiated the chain. The cycle shown in Fig. 1 results in the overall addition of a CH_2 group by the sequential addition of a C–H intermediate followed by subsequent hydrogenation.

The initial alkylidene intermediate has the choice of reacting either with an adsorbed CH intermediate, as was just shown, or with adsorbed hydrogen atoms to form an $R–CH_2$ intermediate, or it can lose a hydrogen atom to form an adsorbed R–C (ethylidynelike intermdiate). This is one of the most stable species that can form (32). The $R–CH_2$ can subsequently react with a second hydrogen atom to form the $R–CH_3$ alkane. This mechanism has some similarities with the mechanism that was proposed by Maitlis *et al.* (36). Two key differences, however, are to be noted. First, the insertion species in this study is adsorbed CH, rather than CH_2. Second, the R–CH–CH alkylidene structure of the growing chain would formally contain a double bond at the atom connected at the surface, but due to the high activity of the surface, the last two carbon atoms of the R–CH–CH chain connect to the surface, thus losing the double bond. Both of the C atoms are now sp^3 hybridized (32).

The alkyl mechanism (mechanism 2), which is shown in Fig. 2, is initiated by an adsorbed $R–CH_2$ intermediate. In the first path through the cycle, R=H, which means that we start with an adsorbed methyl (CH_3) intermediate. The adsorbed $R–CH_2$ species can subsequently react with a coadsorbed CH monomer unit to form an $R–CH_2–CH$ radical surface intermediate. This species can either hydrogenate to form the adsorbed $R–CH_2–CH_2$, which is the homologue of the species we started with, or it can dehydrogenate to form $RCH_2–C$ ethylidynelike intermediate, which is one of the most stable species (32). The initial $R–CH_2$ adspecies can either couple with surface CH intermediates or hydrogenate to form the ($R–CH_3$) alkane product. This mechanism is quite similar to the classical carbene mechanism in the literature. There is one major exception: the monomer which inserts into the growing chain here is an adsorbed CH rather than an adsorbed CH_2.

It is worth mentioning that the two mechanisms share one common intermediate, namely the R–CH species. Because of this, the growing chain can potentially switch between one mechanism and the other in subsequent growth cycles.

In Fig. 3, we show the adsorption energies and the transition state structures for the surface intermediates involved in the first two elementary steps proposed in mechanism 1. In Fig. 4, we show the adsorption structures and energies along with isolated transition states for the second mechanism.

The choice of a common reference energy during the catalytic cycle is not arbitrary, provided that new species are added at their reference energy. "$n\mathrm{CH}_{ads} + n\mathrm{H}_{ads} + \mathrm{H}_{2gas}$" was finally used. The use of gas-phase reactants as references will lead to differences in energies of the same species at the end of one catalytic cycle and at the beginning of the next catalytic cycle.

The transition state for the first elementary step in mechanism 1 (Fig. 3) involves the coupling of an adsorbed CH_2 with an adsorbed CH species to form a surface CH_2CH intermediate. The barrier is 102 kJ × mol^{-1} with respect to separated adsorbed methylene and methine, and 72 kJ × mol^{-1} with respect to methylene and methine coadsorbed at adjacent sites which share a common metal atom. The reaction involves a simultaneous weakening of the metal–carbon bonds at the expense of the formation of the carbon–carbon bond. The transition state structure for this reaction is shown in Figs. 5a and 5b. In the transition state, the CH group is adsorbed at an hcp site with the C–H tilted away from the incoming CH_2 group.

The vinyl intermediate that forms is subsequently hydrogenated in the second step of mechanism 1 to form ethylidene. The activation barrier for this step is quite low. Most of the barrier lies in simply forming the coadsorbed state, whereby hydrogen and vinyl share a single Ru atom. The energy cost for this step is 24 kJ × mol^{-1}. The activation barrier from this neighboring reactant state is only 8 kJ × mol^{-1} to form ethylidene.

The first TS in the second revolution of the cycle for mechanism 1 involves the coupling of adsorbed $CH_3–CH$ with an adsorbed CH to form surface $CH_3–CH–CH$ species. The barrier for this step is 118 kJ × mol^{-1} with respect to separated reactants or 61 kJ × mol^{-1} with respect to reactants coadsorbed at neighboring sites. As might be expected, the barriers are quite similar to those that form vinyl (102 kJ × mol^{-1} for the separated state and 72 kJ × mol^{-1} for the coadsorbed state) in the first pass through mechanism 1.

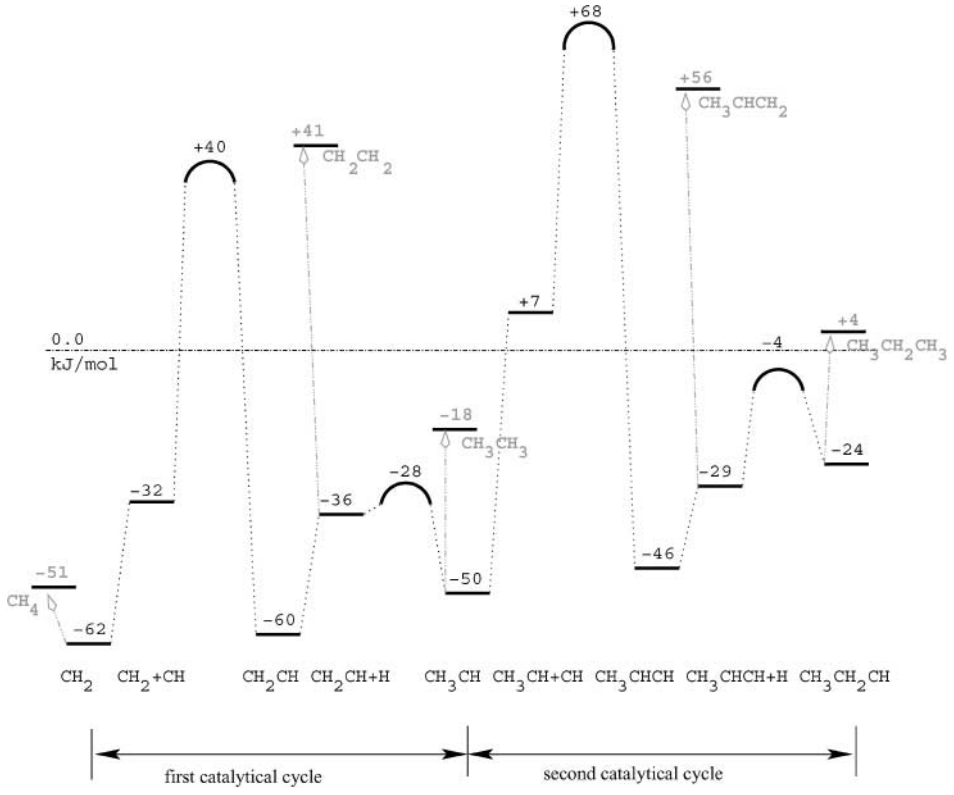

FIG. 3. Fischer–Tropsch, mechanism 1. The first two catalytical cycles, intermediates, transition states, and chain-growth termination.

The 1-propenyl intermediate that forms in this second cycle through mechanism 1 can be hydrogenated to form a surface propylidene. This reaction has a barrier of 25 kJ × mol^{-1} with respect to coadsorbed reactants that sit at adjacent sites and 42 kJ × mol^{-1} if the 1-propenyl and hydrogen atoms are removed from one another. This is the second activation barrier given for the second revolution through mechanism 1 given in Fig. 3.

In the second mechanism (Fig. 4), the first elementary step involves coupling of a surface methyl with a surface methylidyne intermediate to form ethylidene. The barrier for this step is only 6 kJ × mol^{-1} with respect to CH_3 and CH coadsorbed at neighboring sites. Forming this coadsorbed state whereby these species sit at adjacent sites, however, is not easy. Both the CH and the CH_3 are tilted to minimize their steric and electronic repulsions. CH_3 leads to strong steric repulsive interactions with the coadsorbed CH. CH, on the other hand, has repulsive interactions with CH_3 which are the result of strong lateral electronic interactions which occur through the metal (34).

The second step in mechanism 2 is the hydrogenation of ethylidene to form ethyl. The transition state for this reaction, which is shown in Figs. 6a and 6b, involves an insertion of a surface hydrogen into a Ru–C bond. The barrier for this step is 77 kJ × mol^{-1} with respect to separated adsorbed species and 62 kJ × mol^{-1} with respect to the reactants adsorbed at adjacent surface sites which share a single Ru surface atom.

The second revolution of the cycle for mechanism 2 starts with the coupling of adsorbed ethyl and methylidyne intermediates to form propylidene. The barrier for this step is 22 kJ × mol^{-1}. This low barrier is similar to that which was found for ethylidene formation which forms in the first revolution of the cycle.

The final step in the second revolution through cycle of mechanism two involves the hydrogenation of the surface propylidene intermediate to form a surface propyl species. The activation energy for this step is 72 kJ × mol^{-1} with respect to separately adsorbed species and 60 kJ × mol^{-1} with respect to adsorbed reactants at neighboring sites. The transition state structure is shown in Figs. 6c and 6d.

The transition state structures for R–CH and CH coupling and R–CH_2–CH hydrogenation are given in Figs. 5 and 6.

The coupling of CH_2 and CH and the coupling of CH_3CH and CH follow similar reaction paths. In particular the isolated transition states have the same basic structure. One of the C–H bonds from CH_2 and the C–H bond from CH_3CH are slightly activated with C–H bond lengths of 1.14 Å. The other C–H bonds are all about 1.10 Å. The C–Ru bond lengths are 2.30 and 2.07 Å for adsorbed CH_2CH and

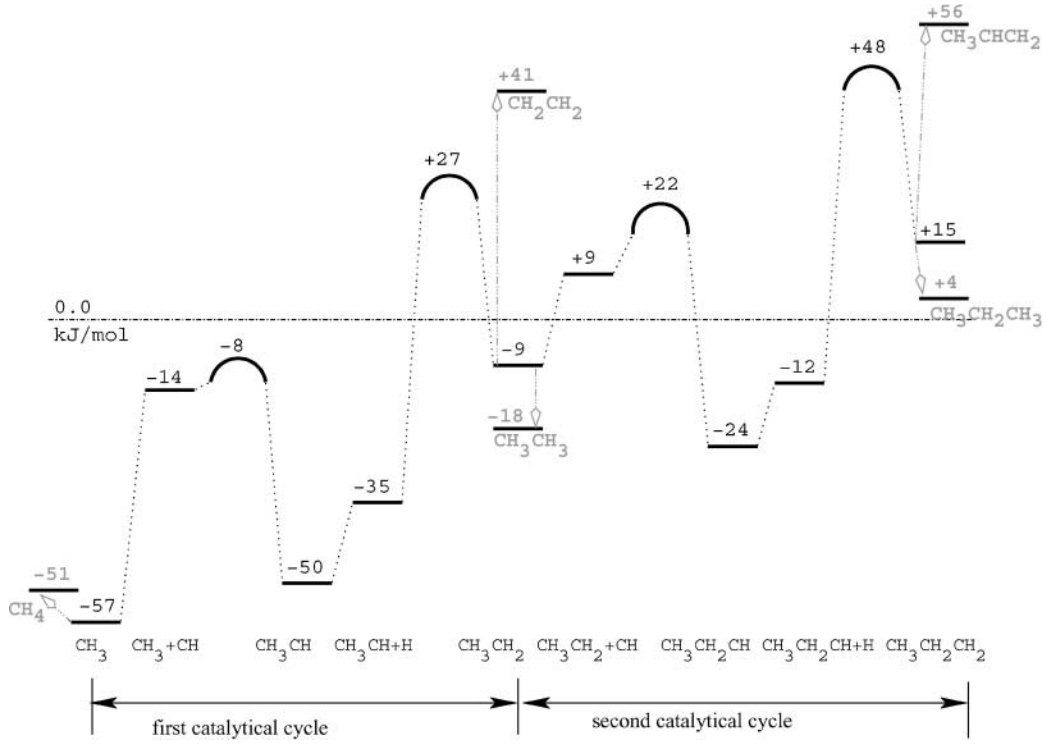

FIG. 4. Fischer–Tropsch, mechanism 2. The first two catalytical cycles, intermediates, transition states, and chain-growth termination.

2.38 and 2.07 Å for adsorbed CH_3CH. The CH group resides in the hcp hollow site where the C–Ru bond lengths are 2.05, 2.04, and 2.29 Å for the CH which couples with CH_2, and 2.05, 2.04, and 2.24 Å for the CH which couples with $CHCH_3$. The C_{CH}–C_{CH-R} is 1.88 Å for R=H and 1.89 Å for R=CH_3 (see Fig. 5).

Similarly, the coupling of CH_3 and CH closely resemble the coupling of CH_3CH_2 and CH. All C–H bonds are 1.10 Å. CH_3 and CH_2CH_3 sit atop, slightly tilted, whereas CH sits at a neighboring hcp hollow site. The C–Ru bond lengths are 2.21 and 2.27 Å for CH_3 and CH_2CH_3 respectively, whereas the C–Ru bond lengths for the CH group are significantly shorter at 1.99, 2.00, and 2.06 Å. The C_{CH}–C_{CH_2R} is 2.60 Å for R=H and 2.66 Å for R=CH_3.

The hydrogenation reactions of CH_2CH and CH_3CHCH have very early transition states. The structures of the vinyl and 1-propenyl intermediates are hardly changed as hydrogen moves from its threefold fcc site to over the top of the active Ru atom to which the CH_2 of vinyl and CH_3CH of propenyl are bound.

The transition states for the hydrogenation of CH_3CH and CH_3CH_2CH are slightly later along the reaction coordinate. The adsorbed CH groups have C–H bond lengths that are about 1.17 Å, and C–Ru bond lengths of 2.14, 2.35, and 2.12 Å. The incoming H atom has a H–Ru distance of 1.66 Å, characteristic for Ru(0001) C–H bond breaking or making (17). The C–H bond which forms after the TS is 1.64 Å for $CH_3CH + H$ and 1.66 Å for $CH_3CH_2CH + H$ (see Fig. 6).

Two termination reactions have to be considered, namely those that lead to the formation of paraffins and olefins. In the first mechanism, olefins can be formed from the hydrogenation of the CH group of the vinyllike R–CH–CH intermediate. This reaction is endothermic. In the second mechanism, olefins can be formed from the dehydrogenation of alkyl intermediates whereby a beta C–H bond is cleaved by the surface. These reactions are also endothermic, but the barriers are expected to be low, since at least one H atom from the beta carbon is slightly activated in the reactant state. The transition state structure for this reaction is expected to be an early one. In fact the endothermicity of these reactions is, to a large extent, controlled by the endothermicity in desorbing the olefin product. The hydrogenation reaction itself is slightly exothermic. We therefore assume that that the barrier is small.

Paraffins can be formed in the first mechanism by two subsequent hydrogen addition steps. If we consider that the barriers for methane formation from CH_2 (17) ($\approx$96 kJ $\times$ mol^{-1}) can be transferred to the R–CH, then the barriers for alkane formation R–CH + 2H $\rightarrow$ R–CH_3 are high even through the reactions are slight exothermic. In the second mechanism, the paraffins can be formed from

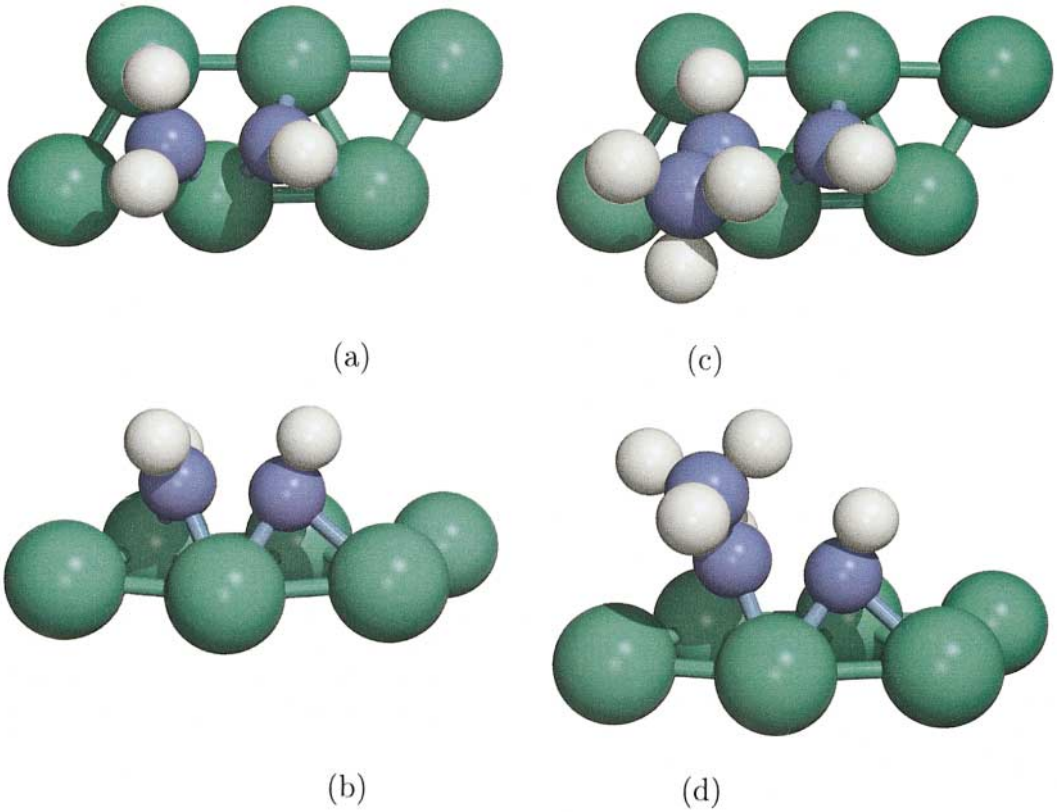

FIG. 5. Transition states for R–CH coupling with CH, R=H (a, b), and CH_3 (c, d); top (a, c) and side (b, d) views.

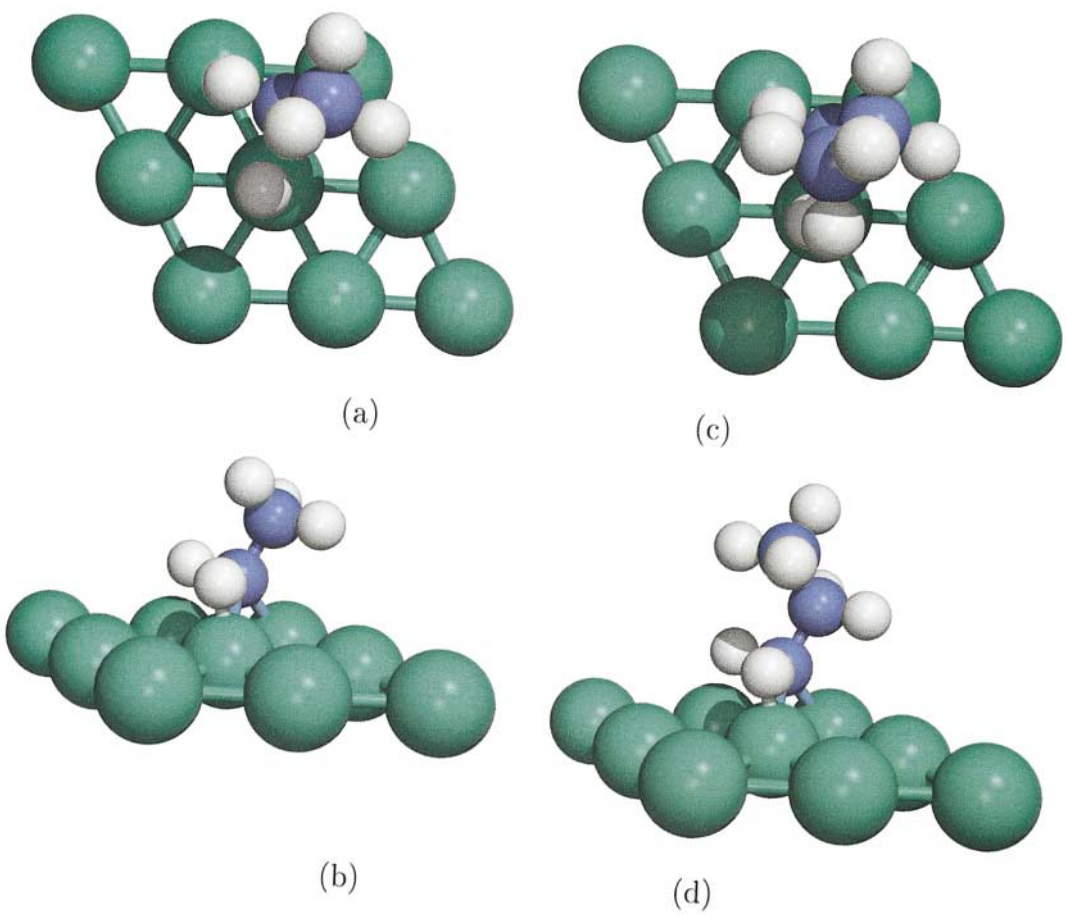

FIG. 6. Transition states for R–CH_2–CH hydrogenation, R=H (a, b), and CH_3 (c, d); top (a, c) and side (b, d) views. The hydrogen atom in shadow in (a) is the one attacking the vinyl group. In (c) the hydrogen atom that is attacking is under one of the hydrogen atoms from CH_3.

alkyls radicals via a single hydrogen addition step. Reasonably high barriers for these reactions are also expected ($\approx$91 kJ $\times$ mol^{-1}).

5. CONCLUSION

We presented two different mechanisms for the propagation sequence involved in hydrocarbon chain growth for Fischer–Tropsch synthesis. Our previous results on the stability of CH_x intermediates on Ru(0001) show that adsorbed CH is the most strongly bound intermediate and may be the most abundant surface intermediates. More definitive results on whether adsorbed CH_2 or CH are the fundamental building blocks, however, will require modeling the delicate balance of hydrocarbon coupling and hydrogenation steps. Preliminary work indicate that the CH species predominates. Herein, we assumed that CH is the monomeric building block.

Since CO dissociation can occur on ruthenium (0001), the Fischer–Tropsch process will not proceed via CO insertion mechanisms. We believe that the O atom is removed as water and the C atom is partially hydrogenated and that it will enter into the C–C coupling cycle.

Both mechanisms examined here were initiated with a hydrocarbon coupling step which was subsequently followed by a hydrogenation step. The key difference between the two mechanisms involves the nature of the "resting state" intermediate of the growing chain. In mechanism 1, we assume that this species is an alkylidene (methylenelike) intermediate. In mechanism 2, the resting state involves an alkyl (methyllike) intermediate. The mobility of the growing chain intermediate on the surface is thought to be higher than that for the CH building block, since CH is so strongly adsorbed.

In the second mechanism, the growing chain intermediates adsorb on Ru(0001) at the final carbon atom in the chain, leaving the CH intermediate with a single-point contact. In the first mechanism, however, some of the intermediates that form prefer to bind to the surface with the last two carbon atoms due to the higher degree of unsaturation.

Since both mechanisms share a common intermediate (R–CH), they can couple through the exchange this intermediate. A growing chain could therefore use either one or the other mechanism for few catalytic cycles. A parallel mechanism is also supported by experimental results.

The hydrogenation of the C_xH_y species that forms involves a reaction coordinate similar to that used for the hydrogenation of CH or CH_2 intermediates on Ru(0001). The incoming H atom sits at a near atop site at the transition state, which results in a Ru–C bond length of 1.66 Å and a H–C bond length of 1.6–1.7 Å.

The C–C coupling in the first mechanism has fairly high barriers, which exceed 100 kJ $\times$ mol^{-1}. The C–C coupling barriers for the second mechanism are significantly lower.

Going from C_1 species to C_{2+} is different in the two mechanisms presented here. The first mechanism shows a small difference in the reaction heat for a catalytic cycle (the stability of CH_2 and homologues is similar), while the reaction heat for a catalytic cycle in the second mechanism is different for the first catalytic cycle (the stability of CH_3 and homologues is much different due to the fact that CH_3 is adsorbed in a fcc threefold hollow site, while the homologues R–CH_2 are adsorbed in a bridge site). This difference could be responsible for the difference observed in experiments for the first coupling (two C_1 species) and the subsequent steps.

The two mechanisms proposed can proceed in parallel. In addition, they can share intermediates, so a hydrocarbon chain can be formed via few cycles of one mechanism and then few from the other, depending on the local concentrations of H atoms (for hydrogenation) and CH group (for C–C coupling). For Ru(0001), TS for C–C coupling are lower that the TS for methanation, which helps to explain why Fischer–Tropsch occurs over ruthenium.

ACKNOWLEDGMENTS

This work is part of the research program of the "Stichting voor Fundamenteel Onderzoek der Materie (FOM)," which is financially supported by the "Nederlandse organisatie voor Wetenschappelijke Onderzoek (NWO)." This work has been accomplished under the auspices of NIOK, the Netherlands Institute for Catalysis Research, Lab Report TUE-2001-5-6. The calculation have been partially performed with NCF support (SC521, MP43a, MP43b).

REFERENCES

1. Anderson, R. B., "The Fischer–Tropsch synthesis," Academic Press, Orlando, 1984.
2. Hindermann, J. P., Hutchings, G. J., and Kiennemann, A., *Catal. Rev.–Sci. Eng.* **35**, 1 (1993).
3. Dry, M. E., *Appl. Catal. A* **138**, 319 (1996).
4. Van der Laan, G. P., and Beenackers, A. A. C. M., *Catal. Rev.–Sci. Eng.* **41**, 255 (1999).
5. Araki, M., and Ponec, V., *J. Catal.* **44**, 439 (1976).
6. Biloen, P., and Sachtler, W. M. H., *Adv. Catal.* **30**, 165 (1981).
7. Brady, R. C., III, and Pettit, R., *J. Am. Chem. Soc.* **103**, 1287 (1981).
8. Baker, J. A., and Bell, A. T., *J. Catal.* **78**, 165 (1982).
9. Van Santen, R. A., De Koster, A., and Koerts, T., *Catal. Lett.* **7**, 1 (1990).
10. Hindermann, J. P., Hutchings, G. J., and Kiennemann, A., *Catal. Rev.–Sci. Eng.* **35**(2), 1 (1993).
11. Brady, R. C., III, and Pettit, R., *J. Am. Chem. Soc.* **102**, 6181 (1980).
12. Ponec, V., and Van Barneveld, W. A., *Ind. Eng. Prod. Res. Dev.* **18**, 26 (1979).
13. Sachtler, W. M. H., *in* "Chemistry and Chemical Engineering of Catalytic Processes" (R. Prins and G. C. A. Schuit, Eds.), p. 583. 1980.
14. Thomas, J. M., and Thomas, W. J., "Principles and Practice of Heterogeneous Catalysis." VCH, Weinheim/New York, 1997.
15. Ciobîcă, I. M., and Van Santen, R. A., submitted for publication.
16. Ciobîcă, I. M., Frechard, F., Van Santen, R. A., Kleyn, A. W., and Hafner, J., *Chem. Phys. Lett.* **311**, 185 (1999).
17. Ciobîcă, I. M., Frechard, F., Van Santen, R. A., Kleyn, A. W., and Hafner, J., *J. Phys. Chem. B* **104**, 3364 (2000).

18. Papoian, G., Nørskov, J. K., and Hoffman, R., *J. Am. Chem. Soc.* **122**, 4129 (2000).
19. Kua, J., and Goddard, W. A., III, *J. Phys. Chem. B* **102**, 9492 (1998).
20. Kua, J., and Goddard, W. A., III, *J. Phys. Chem. B* **103**, 2318 (1999).
21. Watwe, R. M., Cortight, R. D., Nørskov, J. K., and Dumesic, J. A., *J. Phys. Chem. B* **104**, 2299 (2000).
22. Pallassana, V., Neurock, M., *et al.*, *J. Phys. Chem. B* **106**, 1656 (2002).
23. Kresse, G., and Furthmüller, J., *Comput. Mat. Sci.* **6**, 15 (1996).
24. Kresse, G., and Furthmüller, J., *Phys. Rev. B* **54**(16), 169 (1996).
25. Perdew, J. P., "Electronic Structure of Solids' 91," Akademie Verlag, Berlin, 1991.
26. Methfessel, M., and Paxton, A. T., *Phys. Rev. B* **40**, 3616 (1989).
27. Vanderbilt, D., *Phys. Rev. B* **41**, 7892 (1990).
28. Kresse, G., and Hafner, J., *J. Phys. Condens. Matter* **6**, 8245 (1994).
29. Monkhorst, H. J., and Pack, J .D., *Phys. Rev. B* **13**, 5188 (1976).
30. Jónsson, H., Mills, G., and Jacobsen, K. W., *in* "Classical and Quantum Dynamics in Condensed Phase Simulations" (B. J. Berne, G. Ciccotti, and D. F. Coker, Eds.), p. 0. 1998.
31. Pulay, P., *Chem. Phys. Lett.* **73**, 393 (1980).
32. Ciobîcă, I. M., Frechard, F., and Van Santen, R. A., submitted for publication.
33. Ciobîcă, I. M., and Van Santen, R. A., *J. Phys. Chem. B* **106**, 6200 (2002).
34. Ciobîcă, I. M., Frechard, F., Jansen, A. P. J., and Van Santen, R. A., *Stud. Surf. Sci. Catal.* **133**, 221 (2001).
35. Ciobîcă, I. M., Frechard, F., Hermse, C. G. M., Jansen, A. P. J., and Van Santen, R. A., *in* "Surface Chemistry and Catalysis" (A. F. Carley, P. R. Davies, G. J. Hutchings, and M. S. Spencer, Eds.), Chap. 5. Kluwer Academic/Plenum, New York, 2002.
36. Maitlis, P. M., Long, H. C., Quyoum, R., Turne, M. L., and Wang, Z.-Q., *Chem. Commun.* **1**, 1 (1996).